

Energy-Scale Calibration of the Suzaku X-Ray Imaging Spectrometer Using the Checker Flag Charge Injection Technique in Orbit

Midori OZAWA,¹ Hideki UCHIYAMA,¹ Hironori MATSUMOTO,¹ Hiroshi NAKAJIMA,² Katsuji KOYAMA,¹
Takeshi Go TSURU,¹ Masahiro UCHINO,² Hiroyuki UCHIDA,² Kiyoshi HAYASHIDA,² Hiroshi TSUNEMI,²
Hideyuki MORI,³ Aya BAMBA,³ Masanobu OZAKI,³ Tadayasu DOTANI,³
Takayoshi KOHMURA,⁴ Yoshitaka ISHISAKI,⁵ Hiroshi MURAKAMI,⁶
Takeshi KATO,⁷ Takeshi KITAZONO,⁷ Yuki KIMURA,⁷ Kazuki OGAWA,⁷ Shusuke KAWAI,⁷ Koji MORI,⁷
Gregory PRIGOZHIN,⁸ Steve KISSEL,⁸ Eric MILLER,⁸ Beverly LAMARR,⁸ and Marshall BAUTZ,⁸

¹*Department of Physics, Kyoto University, Kita-Shirakawa, Sakyo-ku, Kyoto, 606-8502*
midori@cr.scphys.kyoto-u.ac.jp

²*Department of Earth and Space Science, Osaka University, 1-1 Machikaneyama, Toyonaka, Osaka 560-0043*

³*Institute of Space and Astronautical Science, JAXA, Yoshinodai, Sagami-hara, Kanagawa 229-8510*

⁴*Department of General Education, Kogakuin University, 2665-1 Nakano-Cho, Hachioji, Tokyo 192-0015*

⁵*Department of Physics, Tokyo Metropolitan University, 1-1 Minami-Osawa, Hachioji, Tokyo 192-0397*

⁶*Department of Physics, Rikkyo University, 3-34-1 Nishi-Ikebukuro, Toshima-ku, Tokyo 171-8501*

⁷*Department of Applied Physics, University of Miyazaki, 1-1 Gakuen Kibana-dai Nishi, Miyazaki 889-2192*

⁸*Center for Space Research, Massachusetts Institute of Technology, Cambridge, MA 02139-4307, USA*

(Received 2008 August 15; accepted 2008 September 20)

Abstract

The X-ray Imaging Spectrometer (XIS) on board the Suzaku satellite is an X-ray CCD camera system that has superior performance such as a low background, high quantum efficiency, and good energy resolution in the 0.2–12 keV band. Because of the radiation damage in orbit, however, the charge transfer inefficiency (CTI) has increased, and hence the energy scale and resolution of the XIS has been degraded since the launch of July 2005. The CCD has a charge injection structure, and the CTI of each column and the pulse-height dependence of the CTI are precisely measured by a checker flag charge injection (CFCI) technique. Our precise CTI correction improved the energy resolution from 230 eV to 190 eV at 5.9 keV in December 2006. This paper reports the CTI measurements with the CFCI experiments in orbit. Using the CFCI results, we have implemented the time-dependent energy scale and resolution to the Suzaku calibration database.

Key words: instrumentation: detectors — techniques: spectroscopic — X-ray CCDs

1. Introduction

After the first successful space flight use of the X-ray charge coupled device (CCD) of the SIS (Burke et al. 1993) on board ASCA, the CCD has been playing a major role in imaging spectroscopy in the field of X-ray astronomy. However, the charge transfer inefficiency (CTI) of X-ray CCDs increases in orbit due to the radiation damage; the CTI is defined as the fraction of electrons that are not successfully moved from one CCD pixel to the next during the readout. Since the amount of charge loss depends on the number of the transfers, the energy scale of X-ray CCDs depends on the location of an X-ray event. Furthermore, there is a fluctuation in the amount of the lost charge. Therefore, without any correction, the energy resolution of X-ray CCDs in orbit gradually degrades. In the case of the X-ray Imaging Spectrometer (XIS) (Koyama et al. 2007) on board the Suzaku satellite (Mitsuda et al. 2007) launched on July 10, 2005, the energy resolution in full width at half maximum (FWHM) at 5.9 keV was ~ 140 eV in August 2005, but had degraded to ~ 230 eV in December 2006.

The increase of the CTI is due to an increase in the number of charge traps at defects in the lattice structure of silicon made by the radiation. Since the trap distribution is not uniform, it would be best if we could measure the CTI of each pixel as Chandra ACIS (Grant et al. 2004). In the case of the XIS, however, it is impossible to measure the CTI values of all the pixels, mainly because the onboard calibration sources do not cover the entire field of view of the XIS. Therefore, we use the CTI of each column to correct the positional dependence of the energy scale.

The XIS is equipped with a charge injection structure (Prigozhin et al. 2004; Bautz et al. 2004; LaMarr et al. 2004; Prigozhin et al. 2008) which can inject an arbitrary amount of charge in arbitrary positions. Using this capability, we can precisely measure the CTI of each column (Nakajima et al. 2008). By applying the column-to-column CTI correction, the positional dependence of the CTI corrected energy scale is greatly reduced, and the over-all energy resolution is also improved (Nakajima et al. 2008).

In Nakajima et al. (2008), the results of the CTI correction was mainly based on the ground-based charge in-

jection experiments. In-orbit measurements were limited within one year after the launch. This paper reports more comprehensive and extended in-orbit experiments up to two years after the launch. The results are based on the data with the normal full window mode (Koyama et al. 2007) without a spaced-row charge injection¹ (Uchiyama et al. 2009), and have been implemented to the Suzaku calibration database and applied to all the data obtained with the same mode. All the errors are at the 1σ confidence level throughout this paper unless mentioned.

2. X-Ray CCD with the Charge Injection Capability

2.1. Checker Flag Charge Injection

The XIS is the set of four X-ray CCD camera systems. Three sensors (XIS 0, 2, and 3) contain front-illuminated (FI) CCDs and the other (XIS 1) contains back illuminated (BI) CCD. The XIS 2 sensor became unusable on November 9, 2006. Therefore there are no data for XIS 2 after that day.

The detailed structure of the CCD has been provided in Koyama et al. (2007). In this paper, we define a "row" and a "column" as a CCD line along the *ActX* and *ActY* axes, respectively (see figure 3 in Koyama et al. 2007). In the imaging area, the *ActX* value runs 0 to 1023 from the segment A to D, while the *ActY* value runs from 0 to 1023 from the readout node to the charge injection structure.

The charge injection structure lies adjacent to the top row (*ActY* = 1023) in the imaging area. We can inject charges from $\sim 50 e^-$ to $\sim 4000 e^-$ per pixel; the equivalent X-ray energy ranges from ~ 0.2 keV to ~ 15 keV.

A charge packet generated by an incident X-ray is transferred to the readout node, then is converted to a pulse-height value. We define PH_o to be the original pulse height generated by the X-ray. In the real case, the readout pulse height of the packet (PH') is smaller than PH_o , because some amount of charges is lost during the transfer. To measure the charge loss, we have to know both PH_o and PH' . However, we can usually measure only PH' , and hence it is difficult to obtain PH_o .

Prigozhin et al. (2004) and Prigozhin et al. (2008) reported a technique to solve this problem by the charge injection method, and Nakajima et al. (2008) applied this technique to the XIS. We briefly repeat by referring figure 3 in Nakajima et al. (2008). First, we inject a "test" charge packet into the top CCD row (*ActY* = 1023). Then, after the gap of a few rows, five continuous packets are injected with the same amount of charge of the test packet. The former four packets are called "sacrificial" charge packets, while the last one is called a "reference" charge packet. The test packet loses its charge by the charge traps. On the other hand, the reference packet does not suffer from the charge loss, because the traps are already filled by the preceding sacrificial packets. Thus we can measure the charge loss by comparing the pulse-height

values of the reference charge (PH_{ref}) and the test charge (PH_{test}). The relation between sacrificial charge packets and reference charge packets is described in Gendreau (1995). We can obtain a checker flag pattern by these injected packets in the X-ray image (right panel of figure 3 in Nakajima et al. 2008) because of the onboard event-detection algorithm (Koyama et al. 2007). Therefore in this paper, we call this technique a "checker flag charge injection (CFCI)."

2.2. Formulation of the CTI

A charge packet in the XIS loses its charge during (a) the fast transfer ($24 \mu\text{s pixel}^{-1}$) along the *ActY* axis in the imaging area, (b) the fast transfer along the *ActY* axis in the frame-store region, (c) the slow transfer ($6.7 \text{ ms pixel}^{-1}$) along the *ActY* axis in the frame-store region, (d) the fast transfer to the readout node along the *ActX* axis. The CTI depends on many parameters such as the transfer speed and the number density of the charge traps (Hardy et al. 1998). The frame-store region is covered by the shield and is not exposed to the radiation directly. Furthermore, the pixel size of the frame-store region ($21 \mu\text{m} \times 13.5 \mu\text{m}$) is different from that of the imaging area ($24 \mu\text{m} \times 24 \mu\text{m}$). Thus the number of traps per pixel may be different between the imaging area and the frame-store region. Then we assumed that the four transfers have different CTI values. We examined the transfer (d) by using the calibration source data taken in April 2007, and found no significant decrease of the pulse height along the *ActX* axis. We, therefore, ignore the charge loss in the transfer (d).

We define that i is the transfer number in the imaging area ($i = \text{ActY} + 1$; here, *ActY* is a coordinate value where an incident X-ray generates a charge packet). Then the relation between PH' and PH_o is expressed as,

$$PH'(i) = PH_o(1 - c_a)^i(1 - c_b)^{1024-i}(1 - c_c)^i, \\ \sim PH_o \{1 - i(c_a - c_b + c_c) - 1024c_b\}, \quad (1)$$

where c_a , c_b and c_c are the CTI values in the transfers (a), (b), and (c), respectively. Here we used the fact that the CTI values are much smaller than 1. Thus we can separate the charge loss into i -dependent component (the second term in the right-hand side of equation 1) and constant component (the third term). We therefore substitute the CTI with CTI1 (the former component) and CTI2 (the latter component), which have the CTI values of $c_1 = c_a - c_b + c_c$ and $c_2 = c_b$, respectively. Then equation 1 can be written as

$$PH'(i) \sim PH_o(1 - ic_1 - 1024c_2). \quad (2)$$

Since the CTI values depend on the amount of transfer charge which is proportional to the pulse height, we assume the CTI is described by a power function of the pulse height (Prigozhin et al. 2004) and expressed as

$$c_1 = k_1(PH_o)^{-\beta} \quad \text{and} \quad c_2 = k_2(PH_o)^{-\beta}, \quad (3)$$

where k_1 and k_2 are scale factors for the CTI1 and CTI2, and the index β is common to the CTI1 and CTI2.

¹ After October 2006, the spaced-row charge injection (Uchiyama et al. 2009) has been a normal observation mode, and hence we should use different correction method.

3. Measuring the CTI with the CFCI

We have conducted the CFCI experiments six times in orbit. Effective exposure time for each experiment ranges from a few to ~ 20 ks. The equivalent X-ray energy of the injected charge packets ranges from ~ 0.3 keV to ~ 8 keV. Since June 2006, we injected various amounts of charge in one experiment. The log is summarized in table 1.

In the CFCI experiments, the test charge is injected to the row at $ActY=1023$ ($i=1024$), and hence $PH'(1024) = PH_{\text{test}}$. The reference charge should be equal to the original charge which does not suffer from the charge loss, and hence $PH_o = PH_{\text{ref}}$. Then equation 2 can be written as

$$c_1 + c_2 = \frac{1}{1024} \left(1 - \frac{PH_{\text{test}}}{PH_{\text{ref}}} \right). \quad (4)$$

We determined $c_1 + c_2$ by measuring the ratio $PH_{\text{test}}/PH_{\text{ref}}$ for each column. From equation 3, we can obtain the relation in the CFCI experiments as,

$$c_1 + c_2 = (k_1 + k_2) PH_{\text{ref}}^{-\beta}. \quad (5)$$

The index β and $k_1 + k_2$ were derived by fitting equation 5 to the values of $c_1 + c_2$ obtained with the CFCI experiments with multiple amount of charge injections (multiple PH_{ref} s; Log Number 3–6 in table 1). The mean and standard deviation of the best-fit β of equation 5 averaged over each sensor are shown in figure 1. The mean value of β shows no time variation, and the time averaged values of XIS 0, 1, and 3 are 0.31, 0.22, 0.15 for XIS 0, 1, and 3, respectively. As for XIS 2, there was only one data point, and we obtained $\beta = 0.34$.

If a charge packet has a volume proportional to the number of electrons and is spherically symmetric, the probability that one electron encounters a charge trap is proportional to the cross section of the charge packet. In this case, we can expect $(PH_{\text{ref}} - PH_{\text{test}}) \propto PH_{\text{ref}}^{2/3}$. From equation 4, the CTI value is proportional to $(PH_{\text{ref}} - PH_{\text{test}})/PH_{\text{ref}}$, and hence $\propto PH_{\text{ref}}^{-1/3}$. Thus the simple model is roughly consistent with the observed β values.

Using the results of all the CFCI experiments (Log Number 1–6 in table 1) and above determined β values, we then re-estimated k_1 and k_2 separately. In this process, we assumed k_1/k_2 is equal to c_1/c_2 which was estimated by the 6.4 keV line from the Sgr C region to be 0.67 and 1.5 for the FI and BI CCD, respectively (Nakajima et al. 2008). From this k_1 , we can obtain the final value of c_1 .

Figure 2 shows an example of the distribution of c_1 in July 2006. We can see significant column-to-column dispersion. Figure 3 shows the change of c_1 from July 2006 to September 2007. We can see that the CTI values of all columns increased, but the increasing rate was different from column to column. The results of figures 2 and 3 indicate that the CTI correction at the column level is strongly required. In figure 4, we show the column-averaged c_1 value as a function of time.

Since the CFCI experiments were only sparsely conducted (see table 1), we interpolate the c_1 and c_2 values for the observations of inter-CFCI epochs. As for the de-

termination of the CTI values before the first CFCI experiment, see appendix.

4. Results of the CTI Correction and the Energy Calibration

A CTI correction, which is the conversion of $PH'(i)$ to PH_o , is made with equation 2, where c_1 and c_2 are calculated from equation 3 by using the k_1 , k_2 , and β values determined in section 3.

4.1. Emission Lines for the Calibration

We used the emission lines from the onboard calibration sources, the Perseus cluster of galaxies, and the supernova remnant 1E0102.2–7219. We retrieved the data from the Data Archives and Transmission System² of ISAS/JAXA. All data were acquired with the normal full window mode and the 3×3 or 5×5 editing mode (Koyama et al. 2007). We used the data with the ASCA grades of 0, 2, 3, 4, and 6. As is mentioned in Koyama et al. (2007), a small fraction of the charge in a pixel is left behind (trailed) to the next pixel in the same column during the transfer. All data used in this paper were corrected for the trail phenomenon. The observations are summarized in table 2.

Onboard Calibration Source ^{55}Fe

The calibration source ^{55}Fe produces the Mn I $K\alpha$ line. The theoretical line center energy is 5895 eV (Bearden & Burr 1967; Krause & Oliver 1979). We used the data from August 2005 to April 2007.

The Perseus Cluster of Galaxies

This is one of the X-ray brightest clusters of galaxies in the sky. The X-ray spectrum is that of a thin thermal plasma with the strong $K\alpha$ line of Fe XXV. The plasma temperature changes smoothly from $kT \sim 4$ keV to ~ 7 keV toward the outer region (Churazov et al. 2003), and the center energy of the Fe XXV $K\alpha$ triplet is almost constant (~ 6.56 keV at $z = 0.0176$) within this temperature range. Its radius of $\sim 15'$ can cover the entire field of view of the XIS ($18' \times 18'$). Thus this source is suitable for measuring the positional dependence of the energy scale.

1E0102.2 – 7219

This is one of the brightest supernova remnants in the Small Magellanic Cloud. With the spatial resolution of Suzaku, it can be regarded as a point source. There are many bright emission lines originated from thermal plasma in the X-ray spectrum below 2 keV. These lines are resolved with the XMM-Newton RGS, and the accurate energies of the line centroids are known (Rasmussen et al. 2001). This object has been used by many instruments for the calibration in the low-energy band, and an empirical model to describe the spectrum has been established³. We used this source as the energy-scale calibrator in the low-energy band.

² <http://darts.isas.jaxa.jp/>

³ <http://cxc.harvard.edu/acis/E0102/>

4.2. Positional Dependence of the Energy Scale

For the data of the Perseus cluster of galaxies, we divided the imaging area into four regions along the *ActY* axis, and extracted a spectrum from each region. Then we fitted the spectra in the 5–7.3 keV band with a power-law model and a Gaussian function, and obtained the center pulse height of the FeXXV $K\alpha$ line. Figure 5 shows the center pulse height as a function of *i*. Triangles and circles indicate the data before and after the CTI correction, respectively. We can see no significant *i* dependence after the CTI correction, and this supports the validity of our correction.

4.3. Energy Scale

The goal is to determine a relation of PH_o and X-ray energy E . From the ground experiments, we found that the PH_o - E relation can be expressed as a broken-linear function linked at the Si-K edge energy of 1839 eV (Koyama et al. 2007). We then determined the PH_o - E relation of each segment by using the lines of the calibration sources (Mn I $K\alpha$ line at 5895 eV) and 1E0102.2–7219 ($K\alpha$ lines of O VIII, Ne IX and Ne X around 650–1020 eV).

We show the results after the CTI correction and the PH_o - E conversion. Figure 6 shows measured center energies of the Mn I $K\alpha$ line as a function of time. Each mark in the plot has an effective exposure of more than 60 ks. The mean values of the center energy are 5896.2, 5895.4, 5895.0, and 5895.4 eV for XIS 0, 1, 2, and 3, respectively. The deviation around the theoretical center energy (5895 eV) is 7.8, 4.4, 6.6, and 7.8 eV for XIS 0, 1, 2, and 3, respectively. Therefore, the time-averaged uncertainty of the absolute energy is $\sim \pm 0.1\%$ for the Mn I $K\alpha$ line of the calibration sources.

We also studied the time evolution of the deviation around the theoretical center energy, and the results are shown in figure 7. We can see that the deviation gradually increases with time.

Figure 8 shows the center energy of the O VIII $K\alpha$ line from the 1E0102.2–7219 data. The mean values of the center energy are 652.6, 653.8, 652.7, and 652.8 eV for XIS 0, 1, 2, and 3, respectively. The deviation around the center energy of the empirical model (653 eV) is 1.4, 1.4, 2.3, and 1.1 eV for XIS 0, 1, 2, and 3. Therefore, the uncertainty of the absolute energy is $\sim \pm 0.2\%$ for the O VIII $K\alpha$ line of 1E0102.2–7219.

4.4. Energy Resolution

We examined the energy resolution in FWHM (ΔE) (Koyama et al. 2007) for each sensor; ΔE is common to all segments. We expressed ΔE as

$$\Delta E \text{ (eV)} = \sqrt{\left\{ a \times \left(\frac{E}{5895 \text{ eV}} \right)^b \right\}^2 + (\Delta E_o)^2}, \quad (6)$$

where a and b are time dependent parameters and ΔE_o is the energy resolution determined by the ground experiments and obtained using equation 1 in Koyama et al. (2007). We determined a and b by using the time his-

tory of the calibration sources and 1E0102.2–7219. The ΔE values obtained in this way is incorporated into the redistribution matrix file (RMF).

Figure 9 shows the energy resolution of the Mn I $K\alpha$ line after the column-to-column CTI correction. We also plot the results of the CTI correction, where we used the CTI values averaged over a segment (the column-averaged CTI correction). We can see that the energy resolution is greatly improved by the column-to-column CTI correction. For example, the energy resolution in December 2006 was greatly improved from ~ 230 eV to ~ 190 eV. On the other hand, with the column-averaged CTI correction, the energy resolution is ~ 230 eV and is not significantly improved. In figure 10, we compared the energy resolution of the Mn I $K\alpha$ line with our RMF model. The deviation of the data points around our model is 5.6, 4.9, 3.4, and 6.3 eV for XIS 0, 1, 2, and 3, respectively.

5. Summary

We have conducted the CFCI experiments six times in orbit. The CTI correction has been done with the CFCI results. We calibrated the energy scale of the XIS precisely using the onboard calibration sources and 1E0102.2–7219. Our calibration results have been applied to all the data obtained with the normal full window mode without the spaced-row charge injection. The results of the CFCI experiments and the current calibration status are summarized as follows:

1. We determined the CTI1 and CTI2 values of each column precisely based on the data of the CFCI experiments. We also found that the pulse height dependence of the CTI does not change with time.
2. After the column-to-column CTI correction, we determined the PH_o - E relation. We also modeled the time-dependent energy resolution.
3. The uncertainty of the energy scale is $\pm 0.2\%$ for the O VIII $K\alpha$ line (~ 0.65 keV) of 1E0102.2–7219, and $\pm 0.1\%$ for the Mn I $K\alpha$ line (~ 5.9 keV) of the calibration sources.
4. With the column-to-column CTI correction, the energy resolution at 5.9 keV in December 2006 was greatly improved from ~ 230 eV to ~ 190 eV.

The authors thank all the XIS members for their support and useful information. This work was supported by the Grant-in-Aid for the Global COE Program "The Next Generation of Physics, Spun from Universality and Emergence" from the Ministry of Education, Culture, Sports, Science and Technology (MEXT) of Japan. M.O., H.U., and H.N. are financially supported by the Japan Society for the Promotion of Science. H.M. is also supported by the MEXT, Grant-in-Aid for Young Scientists (B), 18740105, 2008, and by The Sumitomo Foundation, Grant for Basic Science Research Projects, 071251, 2007. H.T. and K.H. were supported by the MEXT, Grant-in-Aid 16002004.

Appendix. Determination of the CTI values before the first CFCI experiment

First, we determined the CTI values of the segments A and D in August 2005. We combined the data of the calibration sources from August 11 to 31, 2005, and obtained the PH' of the Mn I $K\alpha$ line. We also estimated PH_o at 5895 eV from the PH_o-E relation determined by the ground experiments, and obtained the ratio PH'/PH_o . From equation 2, the ratio can be expressed approximately as $PH'/PH_o = 1 - i_{cal}c_1 - 1024c_2$, where i_{cal} is the mean transfer number of the calibration events (typically ~ 900). We determined c_1 and c_2 at 5895 eV from PH'/PH_o with the c_1/c_2 ratio fixed to the values shown in section 3. The c_1 and c_2 for other pulse-height values were calculated from equation 3, where we used the column-averaged and time-averaged β values determined in section 3. Then for segments B and C, we took the average CTI values of the segments A and D. We regard the CTI values obtained in this procedure as those on August 11, 2005 (the day of the XIS first light). Note that these values are determined for each segment, not for each column.

References

- Bautz, M. W., Kissel, S. E., Prigozhin, G. Y., LaMarr, B., Burke, B. E., & Gregory, J. A., 2004, Proc. SPIE, 5501, 111
- Bearden, J. A., & Burr, A. F. 1967, Reviews of Modern Physics, 39, 125
- Burke, B. E., Mountain, R. W., Daniels, P. J., Cooper, M. J., & Dolat, V. S., 1993, Proc. SPIE, 2006, 272
- Churazov, E., Forman, W., Jones, C., Böhringer, H. 2003, ApJ, 590, 225
- Gendreau, K. C. 1995, PhD Thesis (Cambridge: Massachusetts Institute of Technology)
- Grant, C. E., Bautz, M. W., Kissel, S. E., & LaMarr, B. 2004, Proc. SPIE, 5501, 177
- Hardy, T., Murowinski, R., & Deen, M. J. 1998, IEEE Transactions on Nuclear Science, 45, 154
- Koyama, K., et al. 2007, PASJ, 59, 23
- Krause, M. O., & Oliver, J. H. 1979, Journal of Physical and Chemical Reference Data, 8, 329
- LaMarr, B., Bautz, M. W., Kissel, S. E., Prigozhin, G. Y., Hayashida, K., Tsuru, T. G., & Matsumoto, H., 2004, Proc. SPIE, 5501, 385
- Mitsuda, K., et al. 2007, PASJ, 59, 1
- Nakajima, H., et al. 2008, PASJ, 60, 1
- Prigozhin, G. Y., Burke, B. E., Bautz, M. W., Kissel, S. E., LaMarr, B., & Freytsis, M., 2004, Proc. SPIE, 5501, 357
- Prigozhin, G. Y., Burke, B. E., Bautz, M. W., Kissel, S. E., & LaMarr, B. 2008, IEEE Trans. Elec. Device., 55, 2111
- Rasmussen, A. P., Behar, E., Kahn, S. M., den Herder, J. W., & van der Heyden, K. 2001, A&A, 365, L231
- Uchiyama, H., et al. 2009, PASJ, submitted

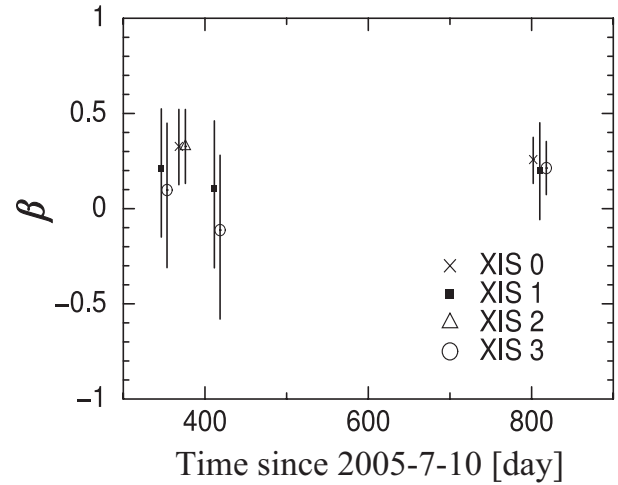


Fig. 1. Time evolution of β averaged over one sensor. We show the standard deviation of β as the error bar.

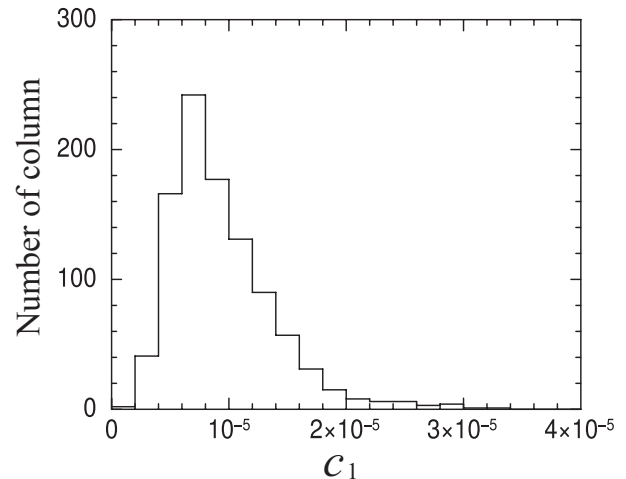


Fig. 2. The number distribution of the CTI1 parameter (c_1). The parameter c_1 is obtained by the checker flag charge injection (CFCI) experiment on July 17, 2006. We show the result of XIS 0 as a typical example. The typical error of c_1 is $\sim 4 \times 10^{-7}$. The mean and the peak (the most probable) values are 9.4×10^{-6} and 6.8×10^{-6} , respectively. The equivalent X-ray energy of the reference charge packet is 4.2 keV.

Table 1. Log of the checker flag charge injection experiments in orbit.

Log Number	Date	Exposure (ks)	The equivalent X-ray energy of the injected charge packets (keV)			
			XIS 0	XIS 1	XIS 2	XIS 3
1	2006/1/17–20	3.7	-	7.1	-	4.6
2	2006/5/20–21	1.2	4.2	-	3.9	-
3	2006/6/26–27	4.9	-	0.3/7.1	-	0.5/4.5
4	2006/7/17	5.7	0.6/4.2/8.0	-	0.6/3.9/7.8	-
5	2006/8/25–26	4.9	-	0.3/7.1	-	0.5/7.0
6	2007/9/28	25.3	0.6/4.1/7.9	0.4/7.2/7.9	-	0.5/4.5/6.5

Table 2. Observational log of the celestial objects.

Object	Obs.ID	Date	Exposure (ks)
The Perseus cluster of galaxies	800010010	2006/2/1–2	50.4
1E0102.2 – 7219	100014010	2005/8/31	24.3
	100044010	2005/12/16–19	59.7
	101005010	2006/4/16	21.3
	101005040	2006/7/17	20.6
	101005070	2006/10/21–22	18.5
	101005100	2007/1/15	22.6
	101005120	2007/3/18–19	18.2

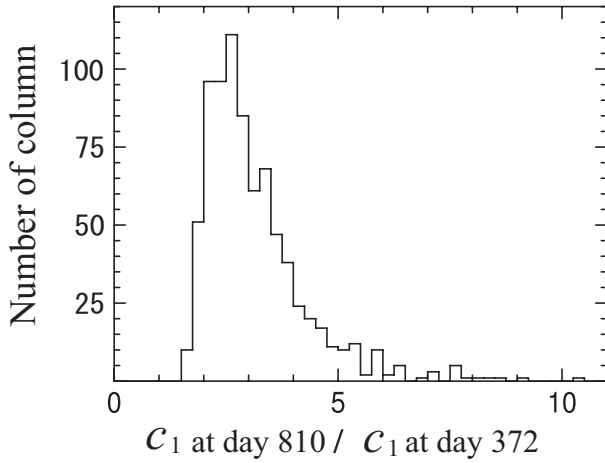


Fig. 3. Same as figure 2, but the ratio of c_1 obtained on July 17, 2006 (372 days after the launch) and on September 28, 2007 (810 days after the launch). The typical error of the ratio is ~ 0.1 . The mean and the peak values are 2.89 and 2.63, respectively. Time evolution of c_1 (increase with time) is clearly seen.

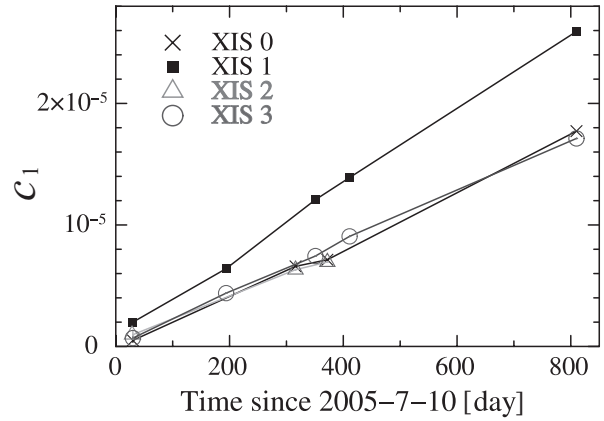


Fig. 4. Time history of column-averaged c_1 at 7.0 keV. We obtained c_1 at day 32 (August 11, 2005) from the calibration sources and that at the other day from the CFCI experiments. We used the relation $c_1 \propto (PH_o)^{-\beta}$ when obtaining c_1 at 7.0 keV. Here we used β shown in section 3.

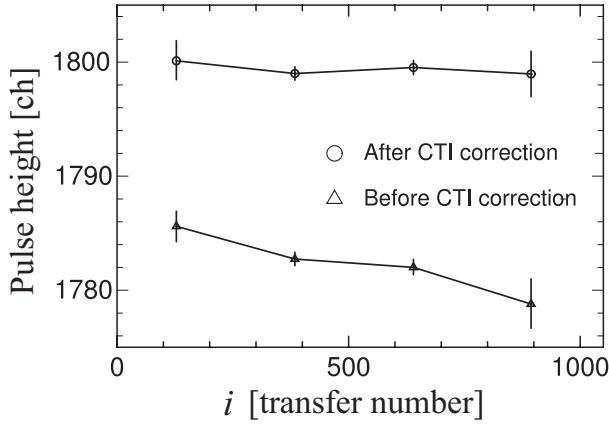


Fig. 5. Transfer number dependence of the center pulse height for the Fe XXV $K\alpha$ line of the Perseus cluster of galaxies. The result of XIS 0 is shown as a typical example. Triangles and circles represent the data before and after the CTI correction, respectively.

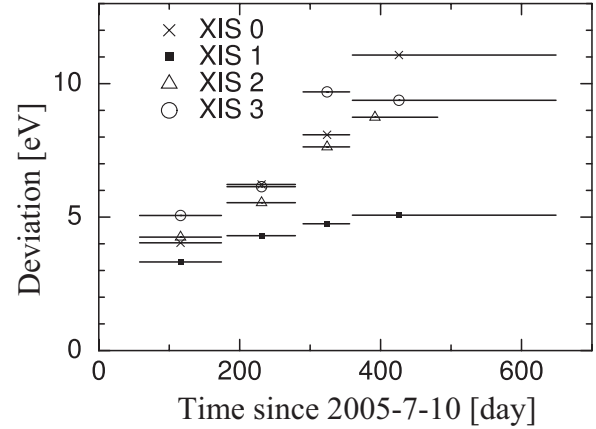


Fig. 7. The deviation of the center energy of the Mn I $K\alpha$ line from the theoretical value (5895 eV) as a function of time. Each mark (except for the last one of XIS 2) is obtained from forty data points of figure 6.

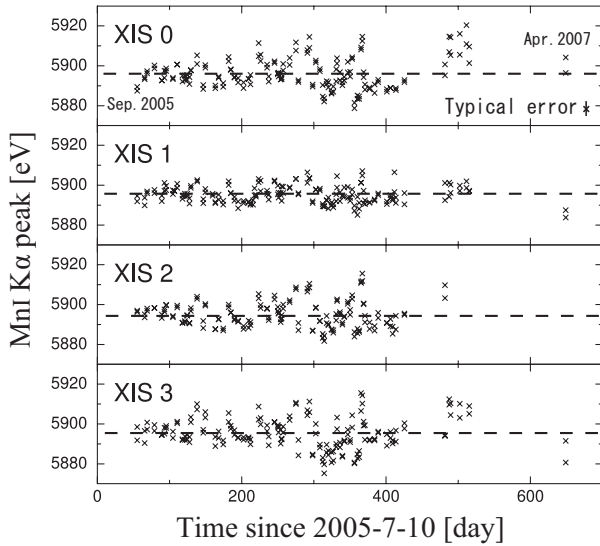


Fig. 6. Center energy of the Mn I $K\alpha$ line for XIS 0-3 after the CTI correction. The theoretical center energy (5895 eV) is shown with dotted lines. Each mark in the plot has an effective exposure of more than 60 ks.

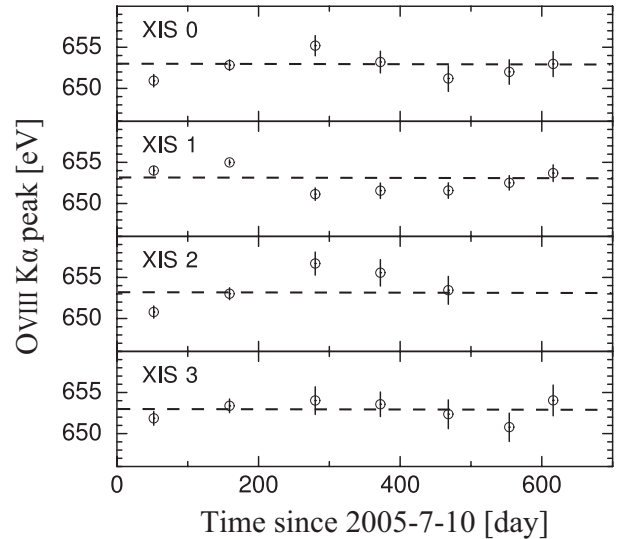
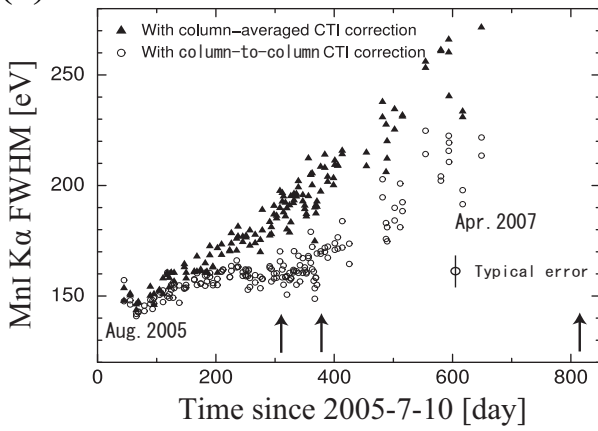


Fig. 8. Center energy of the O VIII $K\alpha$ line from 1E0102.2 – 7219 after the CTI correction. Dotted lines indicate the center energy of the empirical model (653 eV).

(a) XIS 0



(b) XIS 1

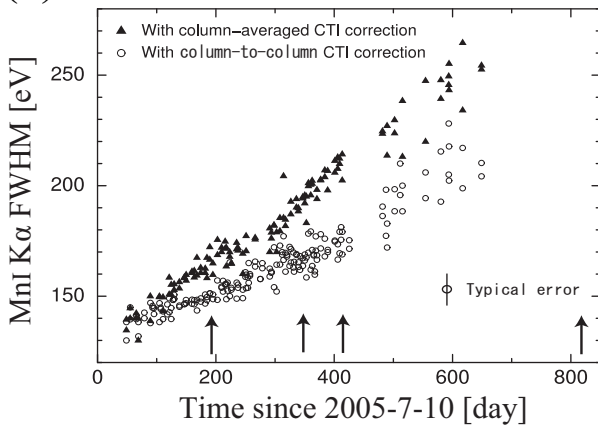


Fig. 9. Comparison of the column-to-column CTI correction (circles) and the column-averaged CTI correction (triangles). We show the energy resolution of the Mn I $K\alpha$ line of XIS 0 (a) and XIS 1 (b). Arrows in the plot indicate the days we performed the CFCI experiments.

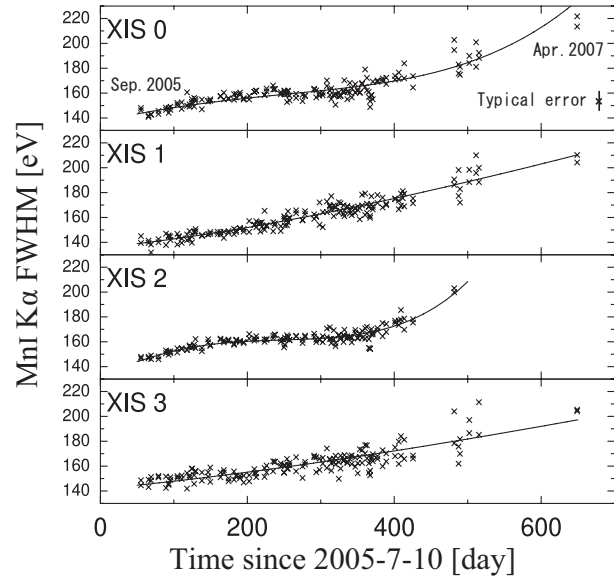


Fig. 10. Energy resolution of the Mn I $K\alpha$ line for XIS 0–3 after the CTI correction. Each mark in the plot has an exposure time of more than 60 ks. The solid lines indicate our model of the energy resolution which is incorporated into the redistribution matrix file.